Journal of Microelectronics and Electronic Packaging (2022) **19**, 25–38

ISSN: 1551-4897

Finite Element Modeling of Rigid-Flex PCBs for Dynamic Environments

John Bell,[1,*] Laura Redmond,[2,3] Kalind Carpenter,[4] and Jean-Pierre de la Croix[5]

ABSTRACT—**Rigid-flex circuit boards are becoming more prevalent as the limits are pushed on the size, mass, and geometry of electronic systems. A key aspect of designing a rigid-flex printed circuit boards (PCB) system is an assessment of the dynamic properties of the PCB and predicting system performance under dynamic loading. Among current modeling methodologies for rigid-flex PCB, a simplified modeling methodology that adequately captures the system dynamics does not exist. This article presents a novel, computationally efficient approach for modeling rigid-flex PCB systems and the calibration of the material models via modal testing. The resulting simplified model is able to capture system frequencies, mode shapes, and representative force-displacement behavior. The proposed methodology is used to model NASA Jet Propulsion Laboratory's Pop-Up Flat Folding Explorer Robot (PUFFER) and assess the sensitivity of a system model to input parameters.**

Keywords—**Rigid Flex PCB, Robotics, Origami Structures, Structural Dynamics, Finite Element Analysis (FEA)**

Introduction

Flexible circuits have significantly expanded the boundaries of design space for electronic devices by permitting circuit geometries previously unthinkable with rigid printed circuit boards (PCB). In designs that involve complex geometries or moving components, the addition of flexible (flex) circuits eliminates the need for connecting cables, allowing for weight reduction, increased durability, space optimization, and improved signal transmittance [1, 2]. Rigid-flex PCB is a hybrid of flexible circuits laminated to conventionally rigid PCB (see Fig. 1). This technology is widely used for manufacturing mobile or wearable devices, military electronics, and medical robotics. Recently, NASA's Jet Propulsion Laboratory (JPL) has created a rigid-flex PCB robot called the Pop-Up Flat Folding Explorer Robot (PUFFER) [3] which utilizes rigid-flex technology. PUFFER is a small, origami-inspired rigid-flex PCB robot that incorporates Nomex^{TM} hinges in addition to flexible circuitry. PUFFER is designed to overcome geologic obstacles and compress to explore hard-to-reach areas (see Fig. 2).

Current literature discussing modeling approaches for rigid-flex PCB is sparse, and those analyzing dynamic properties are an even smaller subset. Rigid-flex PCB systems have additional failure modes compared with traditional PCBs caused by interpanel contact that may cause shearing and frictional forces to develop, thus endangering exposed mounted components. This necessitates dynamic analysis of these systems. Often, modeling methodologies for origami systems (not necessarily just rigid-flex PCB systems) resort to oversimplifications, such as representing the folds by a bar-and-hinge [5] or implementing a simple linearly stiff rotational spring [6]. It is also possible to develop complex, computationally expensive models with more fidelity than required to dynamically characterize such a system by discretely modeling parabolic hinges with initial deformations and strains. Gaps in literature include a standardized approach for efficiently modeling rigid-flex PCB systems, dynamic characterization of these systems, and design considerations informed by the dynamic results. This article proposes a computationally efficient approach for modeling rigid-flex PCB systems for dynamic applications, including the possibility of incorporating Nomex hinges like those found on the PUFFER. A test program of PCB panels with and without Nomex hinges is used to demonstrate material calibration procedures. The sensitivity of the models to damping properties and manufacturing tolerances is also examined. NASA JPL's PUFFER is selected as a case study to demonstrate the proposed modeling technique and parameter sensitivity in the context of a system level model. Finally, guidance for the use of the proposed modeling approach for other rigid-flex PCB systems is provided.

The organization of the remainder of the article is as follows: Literature Review section gives an overview of existing literature on PCB, flex circuit, and fabric modeling, Modeling Methodology section presents the proposed computationally efficient dynamic modeling methodology for rigid-flex PCBs, Material Characterization via Modal Testing section demonstrates the material calibration of the model, Material Damping section discusses the incorporation of damping into the model, PUFFER Case Study section demonstrates the modeling technique and model sensitivity in the context of the system-level model of PUFFER. Finally, Conclusions and Future Work section provides the conclusions of the work, including guidance for the use of proposed modeling approach for other rigid-flex PCB systems.

The manuscript was received on October 15, 2021; revision received on February 22, 2022; accepted on February 28, 2022.

[1]Glenn Department of Civil Engineering, Clemson University, South Palmetto Boulevard, Clemson, South Carolina 29631
[2]Glenn Department of Civil Engineering, Department of Mechanical Engineering, Clemson University, South Palmetto Boulevard, Clemson, South Carolina 29631
[3]NASA Jet Propulsion Laboratory, California Institute of Technology, 4800 Oak Grove Drive, Pasadena, California 91109
[4]Robotic Vehicles and Manipulators Group, NASA Jet Propulsion Laboratory California, Institute of Technology, 4800 Oak Grove Drive, Pasadena, California 91109
[5]Maritime and Multi-Agent Autonomy, NASA Jet Propulsion Laboratory, California Institute of Technology, 4800 Oak Grove Drive, Pasadena, California 91109
*Corresponding author; email: jsb6@clemson.edu

doi:10.4071/imaps.1655356

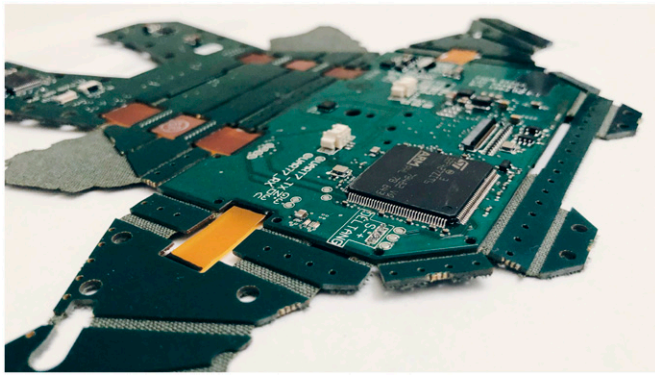

Fig. 1. A rigid-flex PCB system connected by Nomex hinges.

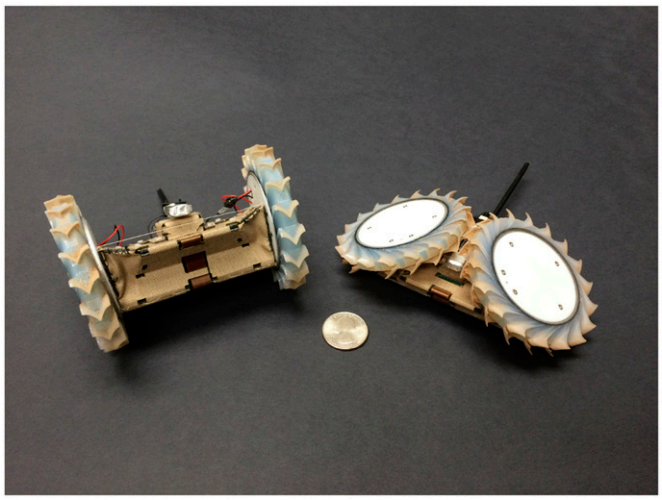

Fig. 2. PUFFER displayed in standard and folded configurations [4].

Literature Review

A. Printed Circuit Board Modeling

PCBs have locally stiffened regions due to large electronic components. The populated components act as lumped masses, and the wide variation in mass and stiffness across the board has a sizeable impact on the dynamic response of the PCB. When applying this to a dynamic finite element model (FEM), it becomes an exercise of balance between model simplicity and satisfactory result accuracy. The appropriate level of detail is determined by analyzing the sensitivities of the PCB to the modeled fidelity of the mounted components. A typical approach is to create a simplified model that gives reasonably accurate results for the particular component. Various methods for simplified PCB models are outlined in Tang et al., and Pitarresi and Primavera [7, 8].

In the most simplistic method, only the base plate material properties are used, and localized stiffness and masses of populating components are ignored. A higher-fidelity model can be constructed by determining the added mass of the populating components and smearing it over the entire board. Global stiffness smearing may also be used by altering the elastic modulus of the board to account for any added stiffness from larger components. Global mass smearing is a common application of mounted components [9]. A higher-fidelity approach is a local mass and stiffness smearing, that has been shown to have adequate results [10, 11]. Local mass smearing can be implemented in several ways; most easily by including elements with higher density to account for the added weight of the component.

The circuit board is populated with sensitive components and delicate solder joints. The solder joints will often fail before the board [12], frequently requiring high-fidelity models to include the individual solder joints. An approach for analyzing solder joint failure is outlined in Gu et al. [13], and will not be discussed in this article. However, the sizeable difference in geometric scale between the solder joints and the base board (FR-4) forces the global element size to be much smaller, increasing run-time and solver complexity. Typically, simplified methods are used for assessing the likelihood of solder joint failure [14, 15].

An additional consideration for modeling PCB is manufacturing tolerances. While these changes from sample to sample may be small, a very slight change in thickness and mass due to adhesives or other fabrication sensitivities can result in substantial changes to dynamic response. These effects are minimized in a rigid-flex system, as the flexible hinges dominate the dynamic system response. For structural components composed of larger PCB sections, these manufacturing tolerance effects will be more prevalent. A rigorous approach to accurately represent PCBs in model space is to determine physical material properties prior to FEM implementation. Other sources of finite element (FE) error stem from PCB parameters that are difficult to determine or implement in model space; namely nonlinear effects and acoustic effects [12].

B.Fabric Modeling

The dynamic behavior of a rigid-flex system is controlled by the properties of the flexible joints. An accurate finite element representation of Nomex fabric is critical to obtain satisfactory system results. Precise finite element modeling of fabric materials can allow for the analysis of thermal properties, impact and failure mechanics, and stress distributions at the individual strand level. These models incorporate the effects of yarn-to-yarn contact and utilize a unit cell implementation methodology [16]. To achieve a high-fidelity model, preliminary fabric analysis is sometimes performed using a scanning electron microscope to determine physical fabric parameters [17]. Individual strands are modeled separately, and boundary conditions and contact parameters are of high importance. This, in turn, often requires a more complex finite element integration scheme and becomes computationally expensive. The authors of this article outline a simpler methodology that adequately captures the dynamic behavior of fabric while maintaining a reasonable computing cost, which becomes of key importance when solving dynamic implicit models.

C. Flexible Circuitry Modeling

Flexible circuitry is a key design point when considering an electronic assembly. In many design applications, industry standards are used, which limit factors such as bend radius or proper routing [18]. With a well-tested ribbon cable and a robust understanding of the mechanical and electrical failure mechanisms, industry standards can confidently ensure the cables will function correctly. In some cases, the behavior

of the flex cable (or other wire-type lines) is examined purely analytically [19-21]. Others result to individually modeling each fiber in a wiring harness [22]. However, the literature lacks simplified modeling approaches for flexible circuitry that could be incorporated within a traditional FEM analysis.

Modeling Methodology

All models were created in HyperMesh and executed in ABAQUS, and constructed to solve in both implicit and explicit environments.

A. Printed Circuit Board

To begin the modal analysis of the PCB samples, a plate element finite element model was constructed as a benchmark against results provided in Arabi and Gracia [23]. The test specimen selected tested by Arabi and Gracia [23] has dimensions of 85 mm x 85 mm x 1.6 mm, with four bolt holes spaced at 67 mm edge-to-edge distance. The modal testing performed had a fixed condition at the bolt holes with a 6 mm diameter. The orthotropic properties used for models in Arabi and Gracia [23] were informed by bend tests. In re-creating a model of the test specimen utilizing a simplified isotropic assumption and an equivalent composite density calculation adequately captures the dynamics of the PCB as shown in Table I and described in detail below. The sample under analysis was found to have consistent in-plane elastic properties, $E_x = E_y =$ 38.5 GPa; this value was assumed for the isotropic elastic model. The benchmarked article has a large difference in frequency values between the 2nd and 3rd modes; however, for a symmetric system, an eigensolution yields two identical modes around the symmetric axis. The authors believe the asymmetry present in the test specimen that did not appear in the FEM was due to localized effects from electronics components. The FEM utilized a smeared mass approach over the entire PCB, as insufficient information was provided to model individual components. For this reason, only the two first modes are used in the benchmark. It is important to note that the data shown represents modes in which a majority of the effective mass manifests. From the comparison of the first two modes, it is evident that a simplified isotropic elasticity stays in reasonable bounds of accuracy. However, if deemed necessary for other applications, an orthotropic material model could be used with little impact on computational speed. The elastic modulus can be further tailored to finely tune dynamic properties as shown in Material Characterization via Modal Testing section.

With the modeling methodology validated, the test samples of PCB were examined. Determining the PCB material parameters was completed using a similar process to one outlined in Arabi and Gracia [23], with the exception of approximating the PCB as isotropic. While an orthotropic model potentially provides a more representative material model, isotropic material properties were sufficient to capture the primary modes of the PCB panels tested. The authors performed a parametric study on the sensitivity of dynamic and stress response between isotropic and orthotropic material models, which indicated very little change to the response of the test panels.

Table I
Arabi [23] Orthotropic Elasticity Versus Bell et al. Isotropic Elastic Model Results

Mode	Arabi [23] modal tested value (Hz)	Arabi [23] orthotropic model (Hz)	Bell et al. isotropic model (Hz)
1	830	844	867
2	1400	1410	1432

For the PCB panels presented in this article, the elastic modulus was initiated at an anticipated lower bound of 24 GPa based on discussions with the manufacturer and calibrated during modal testing of the PCB panels. The FR4 core density was taken as an average of FR4 and polyimide densities (Table II). Using the given layup of the circuit board (Fig. 3), the effective density was calculated and served as an adequate value for initial modeling efforts. This was calculated using eq. (1), which reflects a density calculation that is weighted relative to the thickness of the materials in the composite panel. To minimize the number of alterable material parameters for the model correlation, this number is later adjusted to reflect the measured density of the PCB samples.

$$\rho_{eff} = \frac{t_{Cu}\cdot\rho_{Cu} + t_{FR4}\cdot\rho_{FR4} + t_{Poly}\cdot\rho_{Poly} + t_{Pre}\cdot\rho_{Pre}}{t_{Cu} + t_{FR4} + t_{Poly} + t_{Poly}} \quad (1)$$
$$= 1.992 \times 10^{-6}\ kg\cdot mm^{-3}$$

To model mounted electronic components, the local mass and stiffness smearing approach was implemented. All electronic components with a mass greater than >.1 g were accounted for explicitly. For the components exhibiting larger surface area, the increase in stiffness was accounted for through a rigid beam element implementation, where the beams are attached to a lumped mass, representing the mass of the component (see Fig. 4). The remaining difference in mass from smaller electronic components ≤.1 g each) was accounted for through a smeared mass.

Table II
Material Parameters for PCB Layup Calculation

Layer	Thickness (*mm*)	Density ($kg\ mm^{-3}$)
FR4 core	.406	1.495×10^{-6}
Polyimide core	.025	1.14×10^{-3}
Polyimide prepreg	.508	1.735×10^{-6}
Copper	$4 \times .013$	8.96×10^{-6}

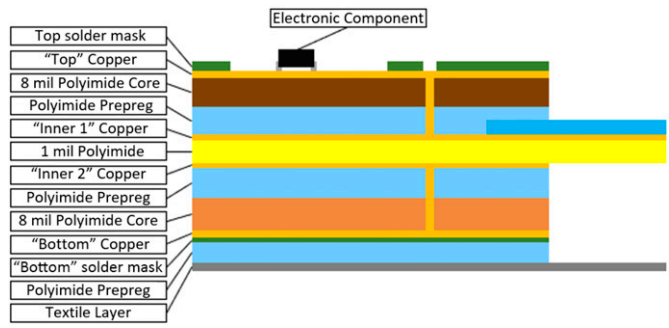

Fig. 3. PCB layup.

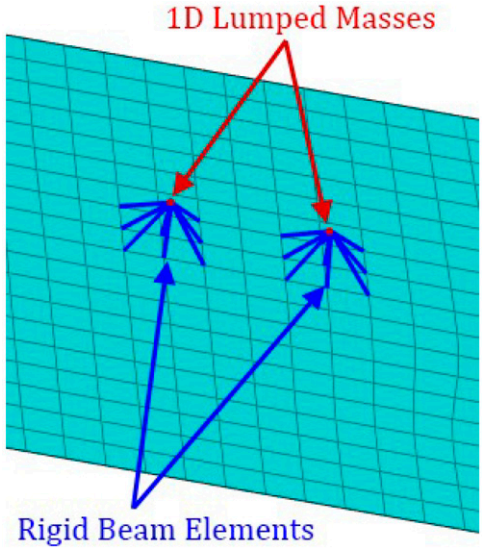

Fig. 4. Local stiffening with rigid R2D2 elements.

The effective density, isotropic modulus, and locally stiffened board simplify the modeling approach while preserving dynamic adequacy in regards to frequencies and mode shapes. Using rigid elements for localized stiffening adds very little computational complexity, but accounts for changes in mode shapes due to component rigidity. Lumping an otherwise complex composite component into a single shell allows for models to be run quickly while maintaining similar dynamic characteristics.

B. Nomex Fabric

Various modeling methodologies were initially investigated to capture the dynamic behavior of Nomex fabric. The objective of the modeling effort was to determine a simplified and dynamically representative finite element procedure. Modeling at yarn-level detail was avoided to retain a reasonable solution time, overall model simplicity, and ease of constructability. Initially, membrane elements and a segmented plate element joint were examined but were not ideal for the simplified modeling method. The membrane joints cannot carry any compression, which is representative of a rigid-flex system. However, the zero-compression property results in numerical difficulties and results in unrealistically soft elements, which fail to account for any axial or bending stiffness the Nomex hinges possess. The segmented plate element joint is constructed of plate elements connected by a series of pins with rotational springs. This method allows for the application of reasonable bending stiffness to the system but is tedious to construct.

The proposed Nomex hinge modeling methodology uses plate elements by modifying the bending rigidity to accurately capture the hinge behavior. From Ashwell [24], we obtain eqs. (2) and (3) for the flexural rigidity D and the axial rigidity R:

$$D=\frac{Et^3}{12(1-\nu^2)} \tag{2}$$

$$R=\frac{Et}{1-\nu^2} \tag{3}$$

Where E is Young's Modulus, t is the plate thickness, and ν is Poisson's Ratio. Eq. (2) is derived from the governing equation of equilibrium of a thin plate in flexure, and eq. (3) is derived from an in-plane stiffness of shells, where $R \approx Et$. In order for the plate element to behave like the Nomex fabric, it is desired to maintain realistic tensile stiffness (R) but have a reduced bending stiffness (D). To accomplish this, the parameters E, t, need to be adjusted proportionally to the material density, ρ, to retain consistent mass. The factor applied can be adjusted according to the desired bending stiffness. To reduce the flexural stiffness of the plate elements by a *flexural stiffness reduction factor*, say δ, the following adjustments are made:

$$E'=E\sqrt{\delta} \tag{4}$$

$$t'=\frac{t}{\sqrt{\delta}} \tag{5}$$

$$\rho'=\rho\sqrt{\delta} \tag{6}$$

Calculating both rigidities and the mass of the plate, we observe a retention of mass and a variable adjustment to the stiffnesses.

$$D'=\frac{E't'^3}{12(1-\nu^2)}=\frac{E\sqrt{\delta}\cdot\left(\frac{t}{\sqrt{\delta}}\right)^3}{12(1-\nu^2)}=\frac{Et^3}{12(1-\nu^2)}=\frac{D}{\delta} \tag{7}$$

$$R'=\frac{E't'}{1-\nu^2}=\frac{E\sqrt{\delta}\cdot\frac{t}{\sqrt{\delta}}}{1-\nu^2}=\frac{Et}{1-\nu^2}=R \tag{8}$$

Let the dimensions of a rectangular plate, the length, width, and thickness, be denoted l, w, and t, respectively, with a given mass m.

Then, accounting for the adjustment in density,

$$V=lwt \;\rightarrow\; m=\rho\cdot lwt \tag{9}$$

$$m'=\rho'\cdot lwt'=\rho\sqrt{\delta}\cdot lw\left(\frac{t}{\sqrt{\delta}}\right)=\rho\cdot lwt=m \tag{10}$$

The largest benefit to the modified plate element joint is that it yields no zero-energy modes and provides confidence in solution convergence. This methodology is simple to construct and allows the user to tailor the material properties to adjust the bending stiffness directly. This computationally efficient modeling methodology assumes linear behavior and neglects nonlinear and second-order effects, thus the appropriate tensile modulus must be selected as the average modulus of the fabric over the model strain range. Unlike Nomex fabric, the modeled joint has the capability to carry compressive forces. However, this primarily occurs when all loads are exactly in-plane with the hinge. For most applications of rigid-flex systems this state is rare, and when it occurs, is quickly passing. Precurving the elements within a Nomex fabric joint helps reduce the possibility of unrealistic compression stresses developing.

A study was performed on the nature of the precurved plate elements to determine the hinge angle at which the compression force carried through the hinge would become significant. This study utilized finite element models of Nomex hinges, with arbitrary width, with a given internal angle between two discrete sections (see Fig. 5). Let the points at which discrete straight-line sections of plate elements meet be denoted the "hinge line." Models were constructed with internal angles at the joints of 180 (straight-line), 150, 120, 90, and 60 degrees, and the same .1 kN force was applied vertically on each model.

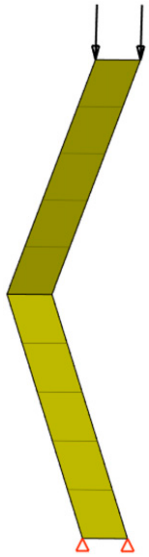

Fig. 5. Modified plate element hinge with 120 degree internal angle.

The elements were given elastic modulus and thickness properties such that the axial rigidity of all plates was 1.0 GPa-mm. Fig. 6 shows plots of the results. As the internal angle degree increases, the vertical displacement exhibited at the top nodes decreases, as the straight-line model simply calculates the axial deformation of the plates. The maximum in-plane principal stress carried by the plate elements exhibit a converse relationship, with the maxi-mum stress being carried in the joints with the smallest predefined internal angle. For these reasons that the authors of the article recommend an assessment of joint motion in the modeling scheme and if any overstiff axial contributions will be made to the model results. If so, it is recommended that the hinge be precurved with several joints with relatively large internal angles, similar to the flex cable benchmark presented.

C. Flexible Circuits

The provided modeling methodology for the Nomex hinges can also be applied to flexible circuitry for dynamic analysis with satisfactory results. This is benchmarked against Wickert [19], a study on dynamic properties of flexible circuitry connecting to the rotating arm in a typical hard drive. The study outlines a hand derivation of the frequency eigensolution calculation with consideration to the deformed position of the cable and substantiates the results through dynamic test results.

The ribbon cable used in the benchmark was modeled with varying mesh densities between three and 60 elements along the length of the spline. The results showing the variation in the frequency of each mode with mesh size are shown in Fig. 7.

The effective elastic modulus was calculated from the cable properties given in the study and lumped masses are included at the end of the cable to account for the inertial properties of the arm. For simplification, out of plane modal displacement is restricted, and it was determined that the effective Poisson's ratio had negligible impact on dynamic results. The Lanczos analysis procedure was used for frequency extraction and residual modes and damping were neglected. The flexural stiffness reduction factor was tuned to best match the experimental frequencies, but iterations of the model were constructed, each with a different flexural stiffness reduction factor and corresponding material properties as shown in Table III.

Table IV summarizes the frequency results for the first six modes, providing the target benchmark frequencies, the extracted FEM frequencies, and the relative error. It was found that a $\delta = 3.5$ yielded the most accurate results. A finer mesh model was then created (4× smaller element sizes) to compare the results.

The simplified plate-element approach has been able to reach results within 20% error for all six modes presented in

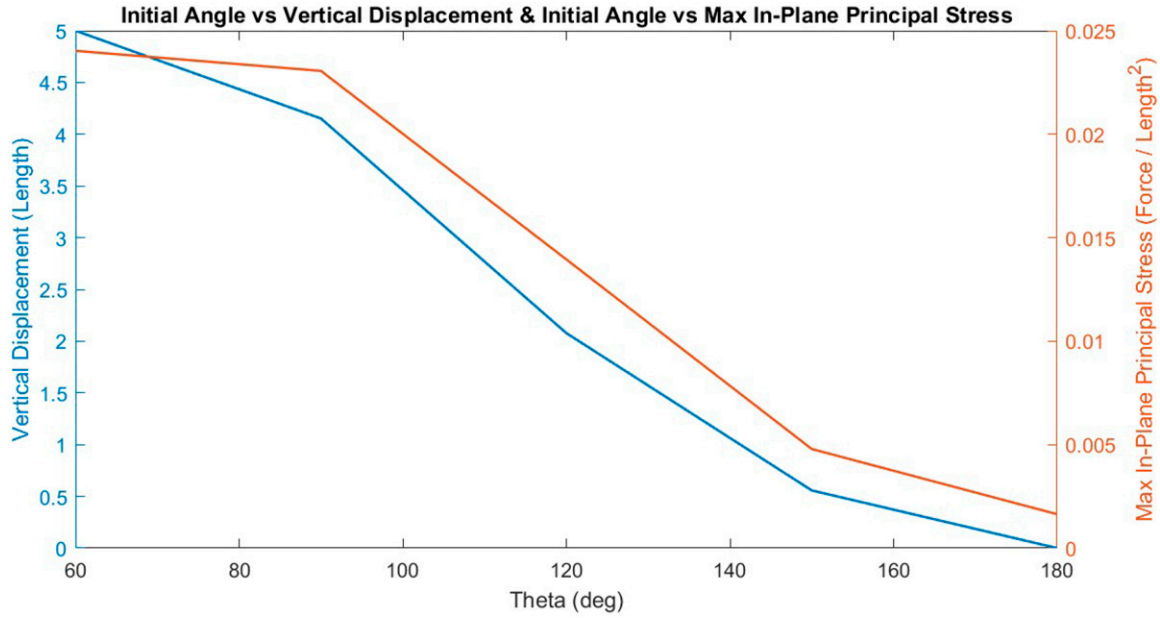

Fig. 6. Stress versus internal angle sensitivity study results.

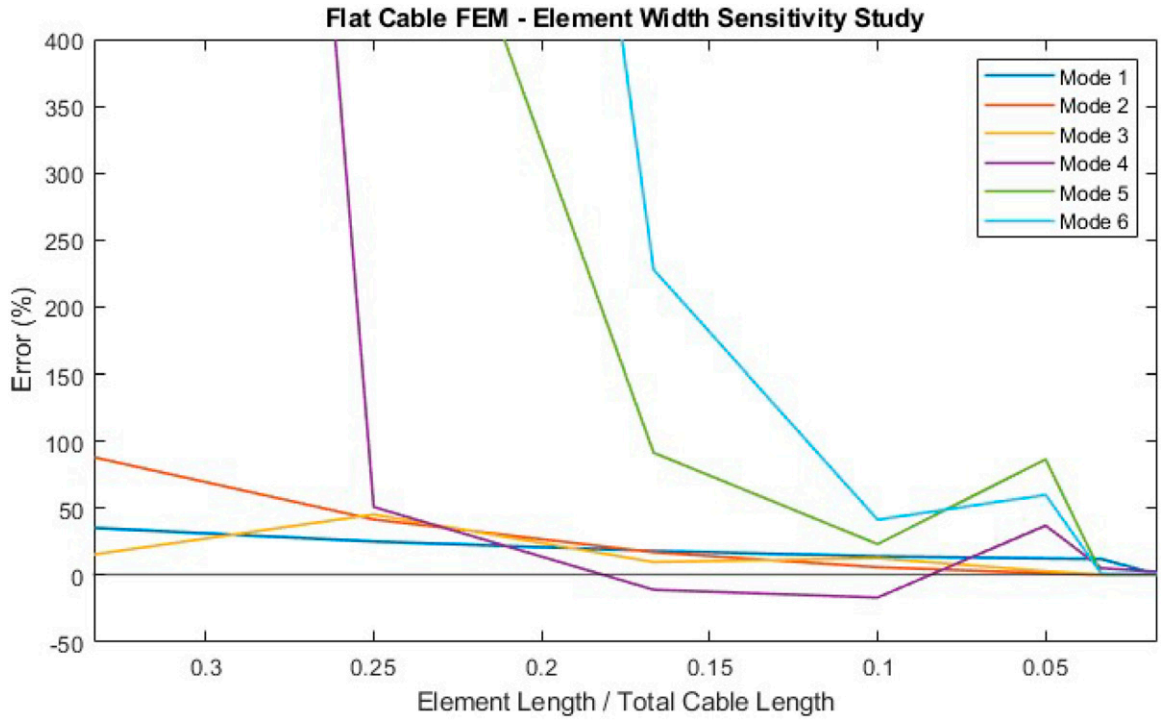

Fig. 7. Sensitivity results on % error against a 10,000 element model.

Table III
Flex Cabling Benchmark Results—Flexural Stiffness Reduction Factor Applied to Material Properties

Flexural stiffness reduction factor (δ):	1.0 (Original)	2.0	3.0	3.5
E (GPa)	27.959	39.539	48.426	52.306
t (mm)	.114	.081	.066	.061
ρ $(kg\ mm^{-3})$	1.898E-06	2.684E-06	3.287E-06	3.551E-06

Table IV
Flex Cabling Benchmark Results

Mode number	Target (Hz)	δ: 3.0—Coarse (Hz)	Err	δ: 3.5—Coarse (Hz)	Err	δ: 3.5—Fine (Hz)	Err
Mode 1	2.86	3.54	54%	3.10	8%	2.91	2%
Mode 2	374	318.62	−15%	303.15	−19%	305.24	−18%
Mode 3	837	784.67	−6%	725.17	−13%	722.87	−14%
Mode 4	1390	1580.70	14%	1460.90	5%	1447.00	4%
Mode 5	2150	2694.90	25%	2490.70	16%	2443.91	14%
Mode 6	3000	4050.20	35%	3623.30	21%	3523.30	17%

the benchmark, and within 2% for the first resonant frequency in which 99.7% of the total mass is participating. Mode shapes and displacements were checked and validated against those presented in Wickert [19].

Material Characterization via Modal Testing

This section discusses the process of determining material proper-ties by dynamic calibration in FEM space to obtained modal test results.

A. Panel Testing

Two different configurations of PCB panels were provided by Pioneer Circuits. The first was a solid board and the second had a single Nomex hinge in the middle, running the full length of the board. Each test coupon was 25.4 mm in length and width and included an extra Nomex layer adhered to the underside. These test panels were fabricated to be consistent with the construction of PUFFER, and both were measured to the nearest .0127 mm and weighed to the nearest .05 g to ensure consistency with the provided layup. The densities were then

calculated based on the observed mass and volume and are outlined in Table V. The panels tested were unpopulated to examine the dynamic response of the panels themselves, and mounted components may be added in model space using the techniques outlined in Printed Circuit Board Modeling section.

The average of the experimentally calculated densities was 10.5% higher than the estimated effective density calculated in Printed Circuit Board section. This was due to an additional Nomex layer not accounted for in the original stackup and manufacturing tolerances.

For all modal tests, uniaxial ceramic accelerometers weighing .8 g were used to collect data. The electrodynamic shaker used had a 25.4 mm peak-to-peak stroke length and was mounted to a sand-filled crate weighing 4.448 N. Local vibrations, deflections of the mounting board, and other data impurities caused by the shaker mount were verified to be insignificant before testing. Accelerometer sensitivity and accuracy checks and amplifier voltage output checks were also performed prior to each test.

1) Solid Printed Circuit Board Testing

Before testing began, an initial model was created as a reference for determining a testing frequency range, understanding the anticipated modal mass participation ratios, and determining the optimum points for accelerometer placement. An initial finite element model of the solid PCB sample was constructed using an average of the thickness measurements for the solid coupons and the lower-bound isotropic modulus of 24 GPa. The boundary conditions for the finite element model were fixed-fixed to represent the conditions of the modal test, which are summarized below. It was found that the majority (92%) of mass participation was accounted for in the first three modes of the panel.

The prime attachment points for the accelerometers were found by calculating the Average Driving Point Residue (ADPR) [25] from the initial FEM results. The solid PCB sample was mounted directly to the shaker using an expander head with drilled aluminum bars fixing both sides of the PCB (see Fig. 8).

The adhesive used to secure the accelerometers was Loctite 451. To best preserve the test coupons though nonabrasive detachment, the accelerometers were mounted to a tape on the surface of the PCB. The tape's adhesion to the PCB was adequate and did not debond during testing. The frequency response function (FRF) reference accelerometer was mounted directly to the expander head, as can be seen in the figure. The torque on all of the bolts was measured, and a sensitivity study on the bolt torque on frequency response was performed. The bolts were torqued such that the boundary conditions were as close to fixed as possible.

Table V
Calculated Densities for PCB Samples

Type solid	Serial no. 16	Density ($kg\ m^{-3}$) 2175.11
Solid	11	2217.29
Solid	12	2152.50
Solid	13	2165.02
Solid	15	2158.96
Solid	14	2180.54
Nomex	7	2245.27
Nomex	8	2258.70
Nomex	9	2226.22
Nomex	10	2236.47
Nomex	5	2243.77
Nomex	6	2239.43

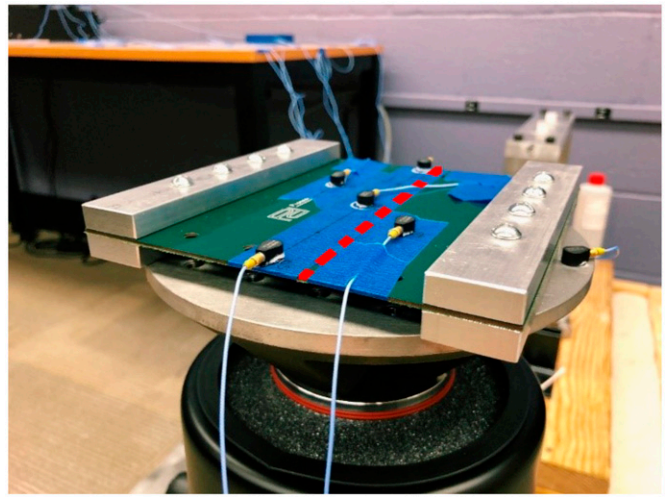

Fig. 8. Mounted solid PCB with a dashed red line indicating the Nomex hinge location on the hinged sample.

Testing was performed both as a sine sweep with a .5 g limit and a random .5 g^2/Hz acceleration from 20 to 2000 Hz with a ramp time short enough to capture any lower-frequency resonances not accounted for by the FEM. A standard Hanning window was applied. Three different PCB samples were tested, each yielding identical mode shapes with very similar frequency results. A final data set for one of the solid samples is pictured below, clearly outlining the presence of the first three modes (Fig. 9). In Figs. 9 and 10, each colored line represents a mounted accelerometer.

2) Nomex Hinge PCB Testing

The testing process and boundary conditions for the PCB coupons with a Nomex hinge was identical to that of the solid test coupons. An initial finite element model was constructed (using the measured average thickness and density) and the frequency test range was determined. The ADPR was extracted from the initial finite element result data, and the accelerometer placement was adjusted accordingly.

The test was run with a sine sweep with a .5 g limit and a random .5 g^2/Hz acceleration from 20 to 400 Hz. Only one prominent mode was under analysis based on mass participation of 91%, hence the frequency bandwidth was shortened to include only this resonance. A Hanning window was applied and a 1 Hz frequency resolution was specified. During testing, effects of nonlinear behavior introduced by the Nomex hinge were minimized by the fixed boundary conditions. Two separate coupons were tested, each yielding very similar frequency and mode shape results. A final set of data are shown in Fig. 10.

In both the solid PCB panels and the panels with the Nomex hinge, the response data are noisy after 400 Hz, as this was the cutoff point. For all data sets, the coherence, phase shift, and spectrum plots were examined to validate the FRF results.

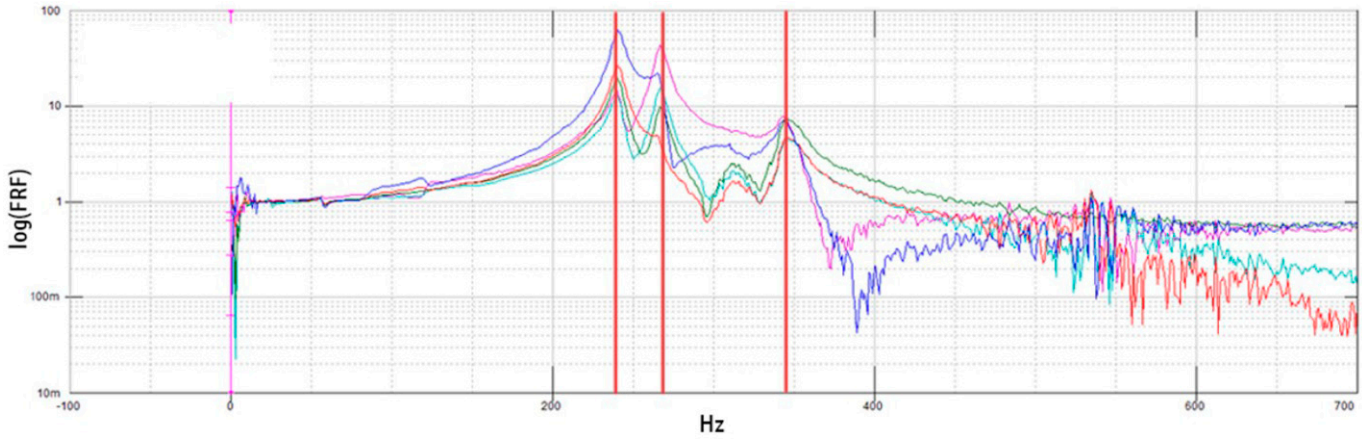

Fig. 9. Frequency (*Hz*) versus log FRF plots for the solid PCB for five mounted accelerometers.

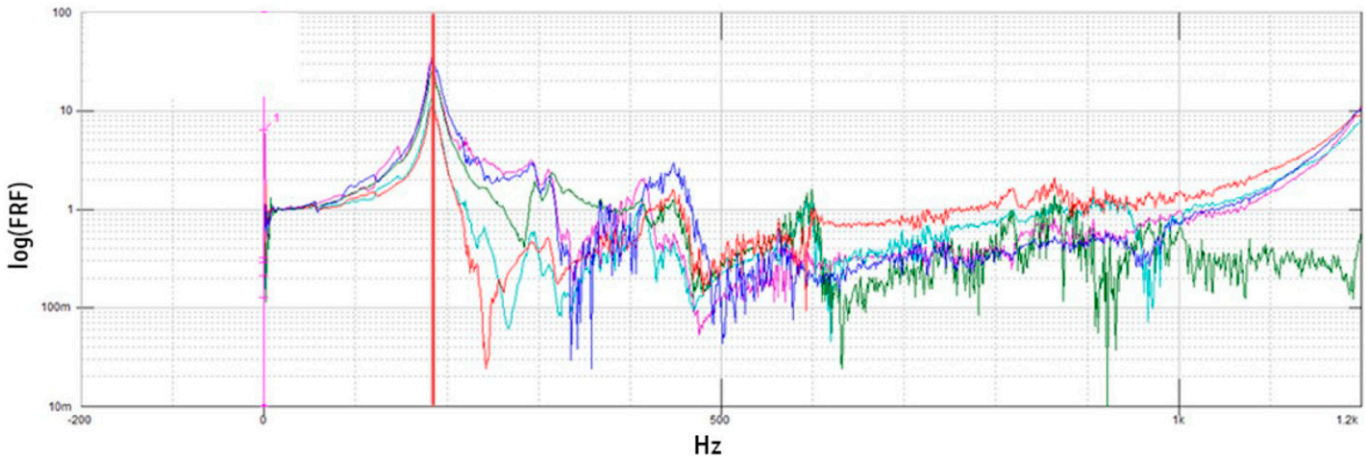

Fig. 10. Frequency (*Hz*) versus log FRF plots for the hinged PCB for five mounted accelerometers.

Animations of the mode shapes were formed directly from the test data to use in the correlation effort.

B. Model Correlation

The finite element model for the solid PCB panel used the same PCB modeling method as outlined in Printed Circuit Board section, with the density adjusted according to its as-measured properties to account for the mass but neglect the stiffness of the Nomex backing. Additionally, accelerometer masses were placed according to the test configuration. To correlate the model, both the resonant frequencies and mode shapes of the relevant modes were considered. Because the thickness and density of the solid PCB FEM were true to the sample tested, the only parameter requiring tailoring was the elastic modulus. The lower bound 24 GPa modulus was adjusted to 25.5 GPa, and the model showed good agreement with the test data with respect to mode shapes and frequencies (see Table VI).

With the new tailored modulus, the only adjustment needed to correlate the model with the Nomex hinge is the bending stiffness of the fabric joint. The hinged PCB model had the same boundary conditions as the solid model and implemented a Nomex hinge with five plate elements spanning the width of the joint (Fig. 11). Table VII outlines the initial Nomex parameters. Poisson's ratio is unavailable from DuPont for Nomex, so the value for Kevlar was used.

Applying a flexural stiffness reduction, δ, factor of 2.25 to modify the Nomex plate elements (Table VIII) correlated the test data with the finite element results. The final tailored material properties are also shown in Table VII. Again, coherence plots, phase shift diagrams, and spectrum diagrams were examined to ensure the physical data were valid.

C. Sensitivity to Solid Printed Circuit Board Properties

In a rigid-flex system, sensitivity of the dynamic response to PCB manufacturing tolerances is less significant than for traditional PCBs but should be considered when the rigid-flex system has large PCB panels exhibiting bending. To illustrate the sensitivity of the dynamic response of the solid PCB to realistic variation of material properties, a parametric study on the solid PCB FEM was conducted, using the correlated material parameters as a baseline. Each parameter listed in Table IX is varied individually to either the upper or lower bound values, while the remaining parameters remain at the correlated values.

Table VI
Solid PCB Coupon Modal Correlation Results

Mode no.	FEM (*Hz*)	Test 1 (*Hz*)	% Error	Test 2 (*Hz*)	% Error	Test 3 (*Hz*)	% Error
1	249.14	247.00	.86%	254.00	1.95%	241.00	3.38%
2	261.37	266.00	1.77%	267.00	2.11%	268.00	2.47%
3	329.83	317.00	3.89%	345.00	4.40%	345.00	4.40%

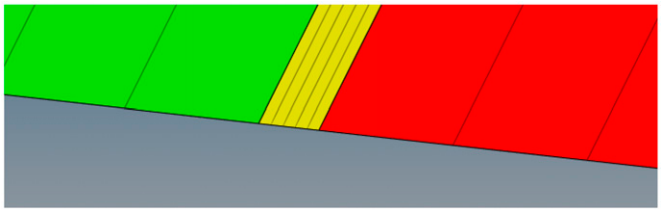

Fig. 11. Modified Nomex hinge plate elements (yellow).

Table VII
Original and Modified Nomex Parameters

Original properties		Tailored properties	
Property	Value	Source	Value
ρ	$1.38 \times 10^{-6}\ kg \cdot mm^{-3}$	[26]	$2.07 \times 10^{-6}\ kg \cdot mm^{-3}$ E
	17 *GPa*	[27]	25.5 *GPa*
ν	.36	[28]	.36
T	.3556 *mm*	Measured	.237067 *mm*

Table VIII
Hinged PCB Coupon Modal Correlation Results

Mode no.	FEM (*Hz*)	Test 1 (*Hz*)	% Error	Test 2 (*Hz*)	% Error
1	183.46	183.00	.3	185.00	.8

The lower bound density value used is the effective density value calculated using the method outlined in Modeling Methodology section. The upper bound value was selected such that the measured density bisects the range. The lower elastic modulus value was chosen as 24 GPa, the initial lower bound value used in the correlation effort. Again, the upper bound modulus value was selected such that the correlated modulus bisects the range of possible values. Arbitrarily low and high values for Poisson's ratio were selected, as this parameter has little effect on dynamic response. The thickness tolerances for the supplied PCB panel were ±.1016 mm and were adjusted about the nominal thickness of the panel. A model sensitivity metric was defined as the % Change in Frequency/% Change in Parameter Value. The results are shown in Figs. 12 and 13.

Upon reviewing the results, it is evident that even small changes in thickness (within the manufacturing tolerances) result in large shifts in panel frequency. Note that the adjustments to the thickness did not include an adjustment to the density to retain identical total mass, but instead reflect the physical case where board thickness is varied but material properties do not change.

Table IX
PCB Parametric Study Property Ranges

Solid PCB parametric study				
Parameter	Lower bound	Upper bound	Correlated value	Units
ρ	1.99×10^{-6}	2.35×10^{-6}	$2.17 \times 10^{-6}\ kg \cdot mm^{-3}$	
E	24	27	25.5	*GPa*
ν	.1	.26	.18	*mm\mm*
T	.775	.958	.857	*mm*

Material Damping

A. Test Setup

This section outlines the modal damping extraction processes and a rigorous parameter selection validation for implementing Rayleigh damping in the model. To begin, the modal damping values were extracted from the FRF test data. To examine the effects of boundary conditions on modal damping, the solid PCB was tested in a free-suspended condition (Fig. 14).

The suspension system was composed of soft elastic bands mounted to a rigid aluminum frame. The lowest relevant resonant frequency of the frame was found to be much higher than the PCB frequencies under analysis, verifying that no localized vibrations would propagate through the suspension system. The stinger was mounted normal to the front PCB face and the results were checked against the FEM with free boundary conditions, which showed good agreement with tested frequencies and mode shapes. Repeats of the free-suspended test were conducted and the test subject was reconfigured to ensure FRF and transfer function symmetry. Damping was calculated using the half-power bandwidth method for both the free suspended test and the clamped boundary test (Fig. 8). Comparing the modal damping values of the first three modes between both configurations, the resulting modal damping of the free-suspended system was significantly higher than the fixed condition. This is expected, as a suspension system introduces additional damping to the test piece [25]. For this reason, and as a conservative estimate, the damping values of the fixed condition were selected as the basis for the Rayleigh damping parameter estimation process. The results of this study are provided in Table X.

Equations used to determine equivalent Rayleigh damping parameters from modal damping values are outlined in several

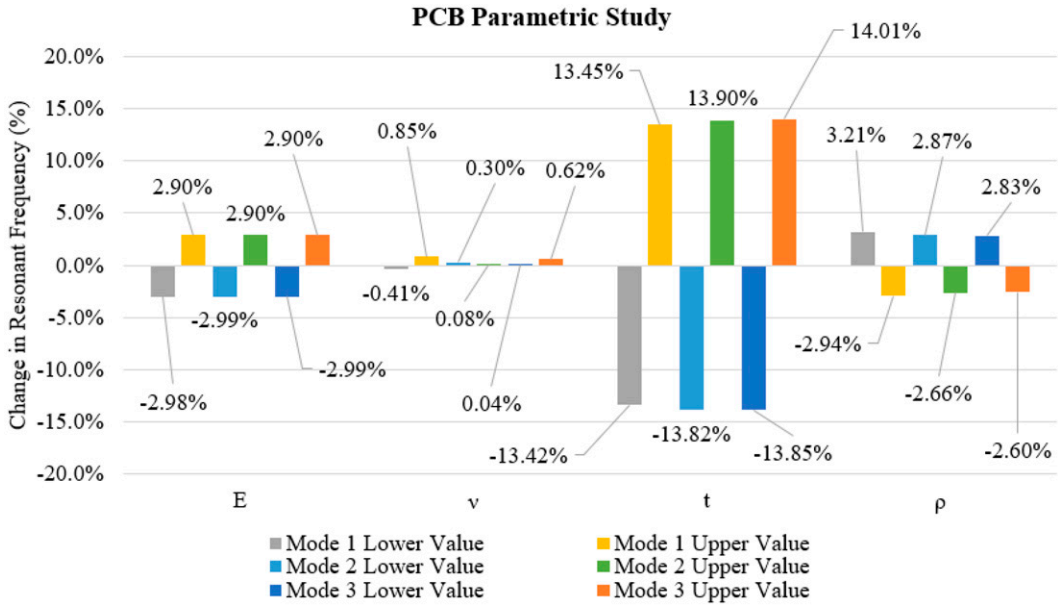

Fig. 12. Parametric study: change in frequency (%) of 1st mode.

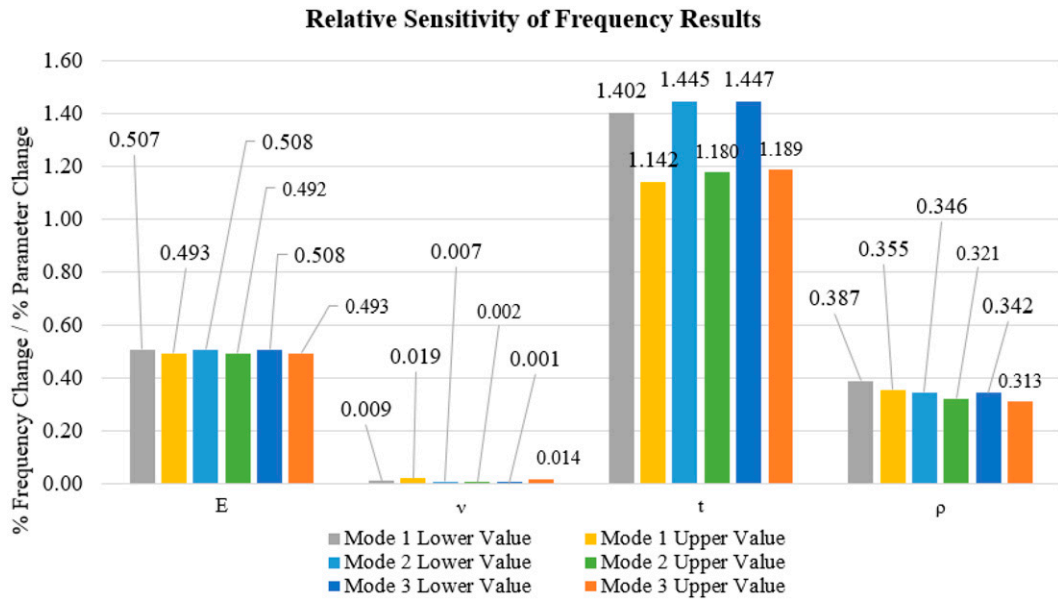

Fig. 13. Parametric study: change in frequency (%) of 2nd mode.

resources [29]. Utilizing the definition of Rayleigh damping defined by Abaqus [30] and the composite mass and stiffness makeup of Rayleigh damping, the following relationship holds, allowing for Rayleigh damping coefficients α and β to be determined by specified modal damping ratios for the *i*th and *j*th modes, respectively.

$$\begin{Bmatrix} \alpha \\ \beta \end{Bmatrix} = \frac{2\omega_i\omega_j}{\omega_j^2 - \omega_i^2} \begin{bmatrix} \omega_j & -\omega_i \\ -1/\omega_j & 1/\omega_i \end{bmatrix} \begin{Bmatrix} \zeta_i \\ \zeta_j \end{Bmatrix} \tag{11}$$

To best-fit the Rayleigh damping curve, the first and third modes (to have a best-fit Rayleigh damping curve along all three modes) of the clamped boundary condition modal test were selected to calculate the Rayleigh parameters using eq. (6). This yielded the solution $\alpha = 10.698$, and $\beta = 1.177\text{E-}05$. The parameters selected yield the following damping curves (Fig. 15). The damping parameters found for the solid PCB were then applied to the PCB in the hinged model. The average modal damping for the hinged PCB test piece was 2.395% and was extracted through testing in the fixed condition. A steady-state dynamic analysis was used to calibrate the

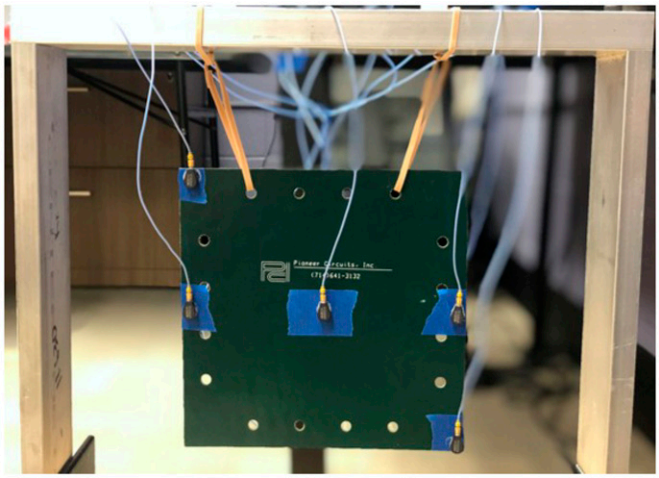

Fig. 14. Free-suspended PCB.

Table X
Averaged Solid PCB Modal Damping Values for Fixed and Free Conditions

Fixed boundary condition		Free boundary condition
Mode no.	Damping	Damping
1	1.26%	2.86%
2	1.82%	2.11%
3	1.54%	1.93%

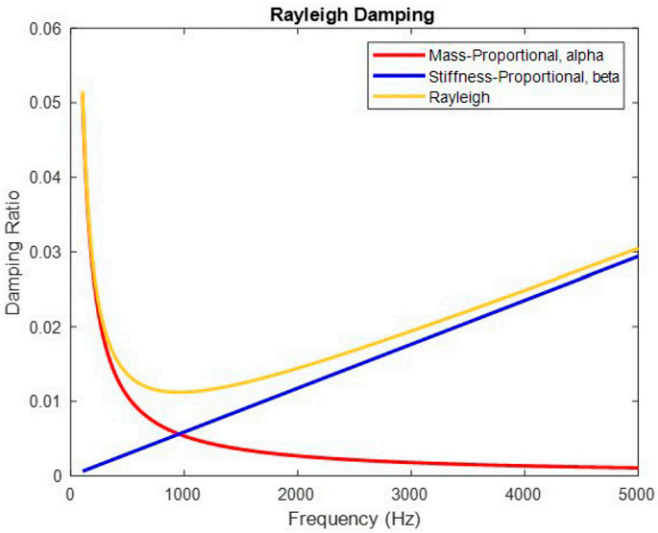

Fig. 15. Rayleigh damping curves for parameters determined for solid PCB sample.

Rayleigh damping parameters for the Nomex fabric hinges. A steady-state dynamic model of the hinged PCB was created, and the solid PCB Rayleigh damping parameters were applied, with zero initial damping applied to the Nomex hinge elements. The half-power bandwidth method, as discussed in Irvine [31], is used to determine damping values from FEM results. The initial steady-state dynamic model resulted in a damping value of 1.176% was calculated for the first resonant frequency. Selecting the Rayleigh damping parameters for the Nomex (to attain the experimental modal damping of 2.395%) was an iterative process. Due to its impact on exclusively low frequency ranges, α was set to 0. Tailoring the stiffness proportional term resulted in a value of β = 8.861E-05. Table XI summarizes the calculated Rayleigh damping parameters for the PCB and Nomex materials.

Table XI
Rayleigh Damping Parameters

Parameter	FR4 PCB	Nomex
α (1/s)	10.698	1.177×10^{-5}
β (sec)	0	8.861×10^{-5}

PUFFER Case Study

To understand the sensitivity of the proposed model in the context of a complex rigid-flex system, the proposed methodology was used to create a model of PUFFER. The PUFFER FEM was constructed in HyperWorks for the ABAQUS standard solver. It is shown in Bell et al. [32] that PUFFER exhibited weak nonlinearities such that traditional modal testing methods may be applied, and the FEM results were able to be correlated to the modal test results with no greater than 15% error between FEM and tested resonant frequencies. A parametric study on the PUFFER rigid-flex system was performed. First, the PCB material properties were individually changed using the same methods discussed in Sensitivity to Solid Printed Circuit BoardPCB Properties section. The results of the shifts in resonant frequency for each PCB material parameter change are shown in Fig. 16. This parametric study assumes all panel properties vary uniformly if they were cut from the same stackup; systems with panels from varying prints need to be examined uniquely. Fig. 17 shows the relative sensitivity of PUFFER's resonant frequency results with respect to percent change in PCB material property value.

The first mode shape of PUFFER has a mass participation that is largely dominated by a single PCB panel. Because of this, the sensitivity of the mode 1 frequency to changes in solid PCB density was significantly greater than other solid PCB parameters. This is true for several other modes PUFFER exhibits, indicating that the accurate mass properties are especially important for regions of a rigid-flex system that exhibit large panel motion.

Having assessed the sensitivity of an assembled rigid-flex system to PCB properties, our attention turns to the dynamic response sensitivity to the Nomex. In this case, a more helpful metric is the sensitivity of the flexural stiffness reduction factor, δ, on frequency results (Fig. 18). This parameter will have increased influence on modal frequencies as the amount of design joint folding increases.

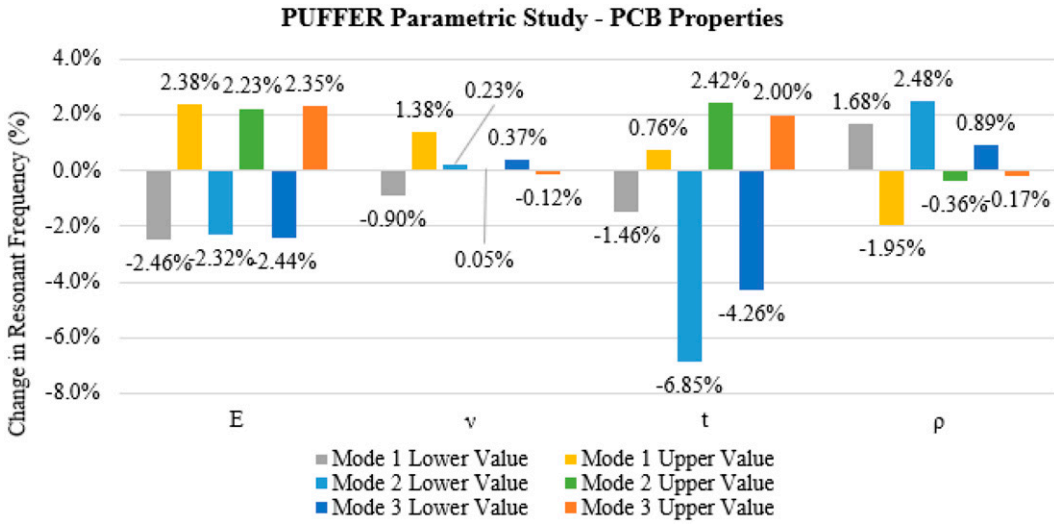

Fig. 16. Summary of the PCB properties on PUFFER's dynamic response.

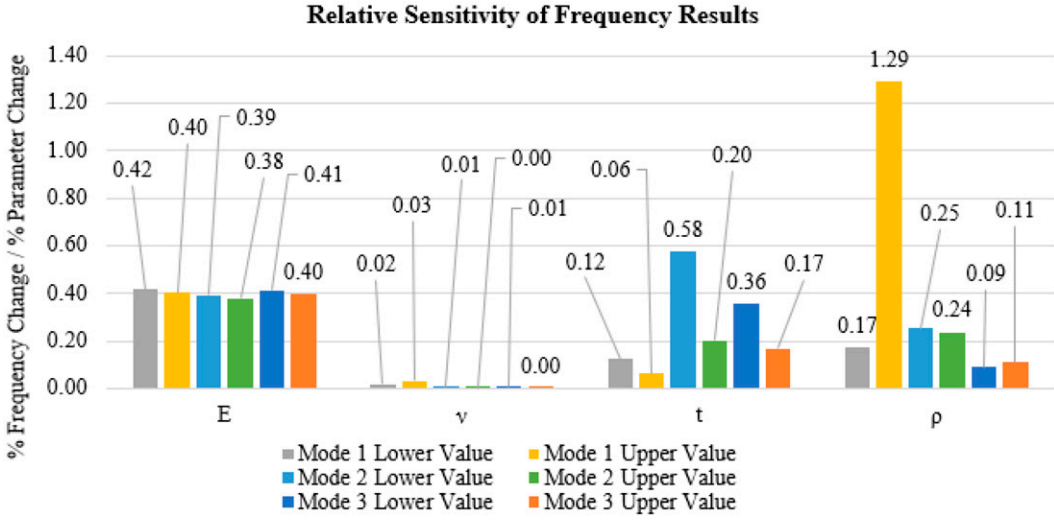

Fig. 17. Summary of relative sensitivity of frequency results.

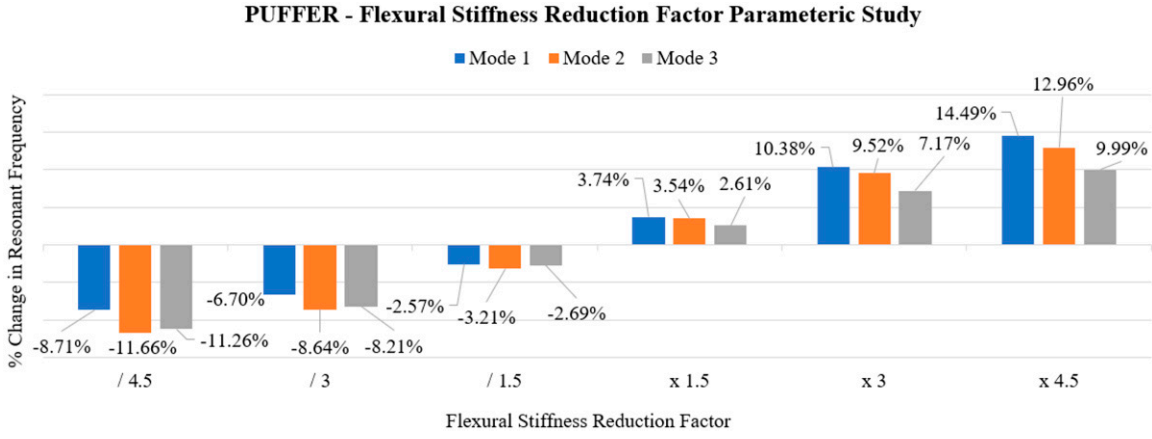

Fig. 18. Flexural stiffness reduction factor parametric study.

Conclusions and Future Work

This article outlined an approach for finite element modeling rigid-flex systems while considering solver run time and dynamic environments. Methodologies were presented for modeling simplified PCB and Nomex components that can be correlated to match modal test results. Sensitives to tailorable parameters were outlined and can be adjusted in order to capture the dynamic behavior of a test specimen through modal testing. The most significant sensitivities are manifest in the joints; in addition to bending stiffness parameters, appropriate joint discretization is key for appropriate model performance.

If a Nomex hinge system is used, it is recommended to precurve the Nomex joint using several elements with relatively large internal angles. Variation in solid PCB material properties within manufacturing tolerances may become a significant for cases that exhibit a large degree of panel bending.

One limitation of the proposed modeling methodology is a capacity for the Nomex or ribbon cable to support axial compressive stresses depending on joint discretization and range of joint motion, which requires additional modeling checks by the user. However, the presented model has significant advantages with regard to run time and model stability over other modeling methods that do not permit any axial compressive stress in these joints. The opinions and drawn conclusions in this article are those of the authors and do not reflect those of the sponsors.

Funding Sources and Acknowledgments

This work was supported by the NASA South Carolina Space Grant Consortium. Grant project numbers are 521383-RP-CM002 (REAP) and 521193-CM001 (GRF). PCB layup information and testing specimens were provided by Dale McKeeby with Pioneer Circuits. The research was carried out with the Jet Propulsion Laboratory, California Institute of Technology, under a contract with the National Aeronautics and Space Administration (80NM0018D0004).

Nomenclature

ρ, Density (kg - mm^{-3})
t, Thickness (mm)
E, Young's Modulus (GPa)
D, Flexural rigidity (kN - mm)
R, Flexural rigidity (kN - mm^{-1})
V, Volume (mm^3)
δ, Stiffness reduction factor
l, Length (mm)
w, Width (mm)
ν, Poisson's ratio
α, Rayleigh damping parameter (s^{-1})
β, Rayleigh damping parameter (s)
ζ, critical damping fraction
ω_n, frequency (rad s^{-1})

References

[1] B.S. Rho, W. Lee, J.W. Lim, K.Y. Jung, K.S. Cha, and S.H. Hwang, "Fabrication and reliability of rigid-flexible optical electrical printed circuit board for mobile devices," *IEEE Photonics Technology Letters*, Vol. 20, No. 12, pp. 964-966, 2008.

[2] T. Rapala-Virtanen and T. Jokela, "New materials and build-up constructions for advanced rigid-flex PCB applications," *Circuit World*, Vol. 31, No. 4, pp. 21-24, 2005.

[3] J.T. Karras, C.L. Fuller, K.C. Carpenter, A. Buscicchio, D. McKeeby, C.J. Norman, C.E. Parcheta, I. Davydychev, and R. Fearing, "Pop-up mars rover with textile-enhanced rigid-flex PCB body," Proceedings of the 2017 IEEE International Conference on Robotics and Automation (ICRA), pp. 5459-5466, Singapore, 2017.

[4] M. Perez, "Origami-inspired robot can hitch a ride with a rover," https://www.nasa.gov/feature/jpl/origami-inspired-robot-can-hitch-a-ride-with-a-rover, May 14, 2020, March 20, 2017.

[5] M. Schenk and S.D. Guest, "Origami folding: a structural engineering approach," *Origami 5*, P. Wang-Iverson, R.J. Lang, M. Yim, Eds., pp. 293-305, Boca Raton, FL, CRC Press, 2011.

[6] R.D. Resch and H. Christiansen, "The design and analysis of kinematic folded plate systems," IASS Symposium. on Folded Plates and Prismatic Structures, Vienna, Austria, September/October, pp. 1-38. Eigentümer, Vienna, Austria, 1970.

[7] W. Tang, J. Ren, G. Feng, and L. Xu, "Study on vibration analysis for printed circuit board of an electronic apparatus," Proceedings of the 2007 International Conference on Mechatronics and Automation, pp. 855-860, Harbin, 2007.

[8] J.M. Pitarresi and A.A. Primavera, "Comparison of modeling techniques for the Vibration analysis of printed circuit cards." *Journal of Electronic Packaging*, Vol. 114, No. 4, pp. 378-383, 1992.

[9] B. de Braz and F.L. Bussamra, "An enhanced random vibration and fatigue model for printed circuit boards," *Latin American Journal of Solids and Structures*, Vol. 14, No. 13, pp. 2402-2422, 2017.

[10] J. Pitarresi, P. Geng, W. Beltman, and Y. Ling, "Dynamic modeling and measurement of personal computer motherboards," Proceedings of the 52nd Electronic Components and Technology Conference 2002. (Cat. No.02CH37345), pp. 597-603, San Diego, CA, 2002.

[11] A. Sayles and T. Stoumbos, "Evaluating the Dynamic Behavior and Analytically Predicted Displacements of Printed Circuit Boards (PCBs) Using the "Smeared-Mass" & Fine Mesh Approach," Proceedings of the 56th AIAA/ASCE/AHS/ASC Structures, Structural Dynamics, and Materials Conference, 2015.

[12] R. Amy, G. Aglietti, and G. Richardson, "Accuracy of simplified printed circuit board finite element models," *Microelectronics and Reliability*, Vol. 50, pp. 86-97, 2010.

[13] J. Gu, D. Barker, and M. Pecht, "Prognostics implementation of electronics under vibration loading," *Microelectronics and Reliability*, Vol. 47, pp. 1849-1856, 2007.

[14] D.S. Steinberg, *Vibration Analysis for Electronic Equipment*, Wiley Interscience Imprint, 2000.

[15] S. Hamasha, Y. Jaradat, A. Qasaimeh, M. Obaidat, and P. Borgesen, "Assessment of solder joint fatigue life under realistic service conditions," *Journal of Electronic Materials*, Vol. 43, No. 12, pp. 4472-4484, 2014.

[16] G. Nilakantan, M. Keefe, T.A. Bogetti, R. Adkinson, and J.W. Gillespie, "On the finite element analysis of woven fabric impact using multiscale modeling techniques," *International Journal of Solids and Structures*, Vol. 47, No. 17, pp. 2300-2315, 2010.

[17] M.O.R. Siddiqui, "Danmei Sun. Finite element analysis of thermal conductivity and thermal resistance behaviour of woven fabric," *Computational Materials Science*, Vol. 75, pp. 45-51, 2013.

[18] NASA Workmanship Standards, *Book 4, section 4.05*, Johnson Space Center, Houston, TX.

[19] J.A. Wickert, "Vibration of Flex Circuits in Hard Disk Drives," *Journal of Vibration and Acoustics*, Vol. 125, No. 3, pp. 335-342, 2003, 10.1115/1.1547661.

[20] C.-C. Chen and J.-Y. Chang, "Modification for the mechanical model of flex cable in hard disk drives with an external electric field," ASME 2013 Conference on Information Storage and Processing Systems, 2013..

[21] K.O. Papailiou, "On the bending stiffness of transmission line conductors," *IEEE Transactions on Power Delivery*, Vol. 12, No. 4, pp. 1576-1588, 1997.

[22] M. Weigelt, C. Thoma, E. Zheng, and J. Franke, "Finite-element-analysis of the mechanical behavior of highfrequency litz wire in flat coil winding," *Production Engineering*, Vol. 14, No. 5-6, pp. 555-567, 2020.

[23] F. Arabi and A. Gracia, "J. -. Dele'tage and H. Fre'mont, Vibration test and simulation of printed circuit board," Proceedings of the 19th

International Conference on Thermal, Mechanical and Multi-Physics Simulation and Experiments in Microelectronics and Microsystems (EuroSimE), pp. 1-7, Toulouse, 2018.
[24] D. Ashwell, "Theory and analysis of plates. Rudolph Szilard. Prentice-Hall, New Jersey. 1974. 724 pp.," The Aeronautical Journal (1968), Vol. 79, No. 770, p. 98, 1975.
[25] D.J. Ewins, "*Modal testing: Theory, practice, and application*. Research Studies Press, Baldock, Hertfordshire, England, 2000.
[26] DuPont. Technical guide for NOMEX brand fiber, July 2001.
[27] M. Jassal and S. Ghosh, "Aramid fibres—an overview," *Indian Journal of Fibre and Textile Research*, Vol. 27, pp. 290-306, 2002.
[28] DuPont. Kevlar Aramid Fiber Technical Guide, 2017.
[29] Z. Song and C. Su, "Computation of Rayleigh damping coefficients for the seismic analysis of a hydro-Powerhouse," *Shock and Vibration*, Vol. 2017, pp. 1-11, 2017.
[30] A. Abaqus, *6.14 Online Documentation,* Dassault Systems, Providence, RI, 2014.
[31] T. Irvine, "The half power bandwidth method for damping calculation," *Isolation*, pp. 1-8, 2005.
[32] J. Bell, L. Redmond, K. Carpenter, and J.-P. De la Croix, "Experimental dynamic characterization of rigid-flex PCB systems," *Journal of Experimental Mechanics*, n.d., Under Review.